ロセスを検討するための iPS 細胞品質管理室）の設備整備を実施した。また、中核機関と共有すべきデータ情報について、申請者と意見交換を行なった。ドナーリクルートのための同意説明文書、研究計画書等の書類整備を進めた。さらに、iPS 細胞製造のための手順書や使用試薬について GMP に準拠する書類についても整備を進めた。

D．健康危険情報
特になし

E．研究発表
特になし

F．知的財産権の出願・登録状況（予定を含む。）
1. 特許取得
該当なし
2. 実用新案登録
特になし
3. その他
特になし

III. 研究成果の刊行に関する一覧表

研究成果の刊行に関する一覧

雑誌

岡野　栄之

発表者氏名	論文タイトル名	発表誌名	巻号	ページ	出版年
Nori S, Okada Y, Yasuda A, Tsuji O, Takahashi Y, Kobayashi Y, Fujiyoshi K, Koike M, Uchiyama Y, Ikeda E, Toyama Y, Yamanaka S, Masaya N, Okano H.	Grafted human induced pluripotent stem cell-derived neurospheres promotes motor functional recovery after spinal cord injury in mice.	Proc.Natl.Acad.Sci. USA	108(40)	16825-30	2011
Yagi T, Ito D, Okada Y, Akamatsu W, Nihei Y, Yoshizaki T, Yamanaka S, Okano H, Suzuki N.	Modeling familial Alzheimer's disease with induced pluripotent stem cells.	Hum Mol Genet.	20(23)	4530-39	2011
Renault-Mihara F, Katoh H, Ikegami T, Iwanami A, Mukaino M, Yasuda A, Nori S, Mabuchi Y, Tada H, Shibata S, Saito K, Matsushita M, Kaibuchi K, Okada S, Toyama Y, Nakamura M, Okano H.	Beneficial compaction of spinal cord lesion by migrating astrocytes through glycogen synthase kinase-3 inhibition.	EMBO Mol Med.	3(11)	682-96	2011
Fujioka M, Tokano H, Fujioka-Shiina K, Okano H, Edge A.S.	Cre/lox mediated in vivomosaic cell ablation to generate novel models for early stages of degenerative disease and tissue repair.	J. Clin. Invest.	121(6)	2462-2469	2011
Kubota Y, Hirashima M, Takubo K, Nagoshi N, Kishi K, Murakami M, Shibuya M, Takakura N, Okano H, Suda T.	Isolation and function of mouse tissue resident vascular precursors marked by myelin protein zero.	J. Exp. Med	208(5)	949-960	2011
Ishizuka K, Kamiya A, Oh EC, Kanki H, Sehadri S, Robinson J, Murdoch H, Dunlop AJ, Kubo KI, Furukori K, Huang B, Zeledon M, Hayashi-Takagi A, Okano H, Nakajima K, Houslay MD, Katsanis N, Sawa A.	DISC1-dependent switch from progenitor proliferation to migration in the developing cortex.	Nature	473(7345)	92-96	2011
Nagoshi N, Shibata S, Nakamura M, Mabuchi Y, Matsuzaki Y, Toyama Y, and Okano H	Schwann Cell Plasticity After Spinal Cord Injury Shown by Neural Crest Lineage Tracing.	Glia	59(5)	771-84	2011
Sawamoto K, Hirota Y, Alfaro-Cervello C, Soriano-Navarro M, He X, Hayakawa-Yano Y, Yamada M, Hikishima K, Tabata H, Iwanami A, Nakajima K, Toyama Y, Itoh T, Alvarez-Buylla A, Garcia-Verdugo JM, and Okano H	Cellular composition and organization of the subventricular zone and rostral migratory stream in the adult and neonatal common marmoset brain.	J. Comp. Neurol.	519(4)	690-713	2011

Matsui T, Takano M, Yoshida K, Soichiro Ono, Fujisaki C, Matsuzaki Y, Toyama Y, Nakamura M, Okano H, Akamatsu W.	Neural stem cells directly differentiated from partially reprogrammed fibroblasts rapidly acquire gliogenic competency.	Stem Cells.	In Press		2012
Ohta S, Misawa A, Fukaya R, Miyoshi H, Okano H, Kawakami Y, Toda M.	Macrophage migration inhibitory factor (MIF) promotes cell survival and proliferation of neural stem/progenitor cells.	J Cell Sci.	In Press		2012
Muto J, Imai T, Ogawa D, Nishimoto Y, Okada Y, Mabuchi Y, Kawase T, Iwanami A, Mischel PS, Saya H, Yoshida K, Matsuzaki Y, Hideyuki Okano H.	RNA-binding protein Musashi1 modulates glioma cell growth through the post-transcriptional regulation of Notch and PI3 kinase/Akt signaling pathways.	PLoS ONE	In Press		2012
Hara-Miyauchi C, Tsuji O, Hanyu A, Okada S, Yasuda A, Fukano T, Akazawa C, Nakamura M, Imamura T, Matsuzaki Y, Okano HJ, Miyawaki A and Okano H.	Bioluminescent system for dynamic imaging of cell and animal behavior.	Biochem Biophys Res Comun	Epub ahead of print		2012
Nakamura-Ishizu A, Kurihara T, Okuno Y, Ozawa Y, Kishi K, Goda N, Tsubota K, Okano H, Suda T, Kubota Y.	The formation of an angiogenic astrocyte template is regulated by the neuroretina in a HIF-1-dependent manner.	Dev. Biol.	363 (1)	106-114	2012
Lin ZY, Imamura M, Sano C, Nakajima R, Suzuki T, Yamadera R, Takehara Y, Okano HJ, Sasaki E, Okano H.	Molecular signatures to define spermatogenic cells in common marmoset (*Callithrix jacchus*).	Reproduction	Epub ahead of print		2012
Okano H, Nakamura M, Yoshida K, Okada Y, Tsuji O, Nori S, Ikeda E, Yamanaka S, Miura K.	Steps toward safe cell therapy using induced pluripotent stem cells.	Circulation Research	In Press		2012
Kawahara H, Imai T, Okano H.	MicroRNAs in neural stem cells and neurogenesis.	Frontiers in Neurogenesis	In Press		2012

雑誌

中辻　憲夫

発表者氏名	論文タイトル名	発表誌名	巻号	ページ	出版年
Aizawa, E., Hirabayashi, Y., Iwanaga, Y., Suzuki, K., Sakurai, K., Shimoji, M., Aiba, K., Wada, T., Tooi, N., Kawase, E., Suemori, H., Nakatsuji, N. and Mitani, K.	Efficient and accurate homologous recombination in hESCs and hiPSCs using helper-dependent adenoviral vectors	Molecular Therapy	In press	In press	2012
Hasegawa, K., Yasuda, S., Teo, J.-L., Nguyen, C., McMillan, M., Hsieh, C.-L., Suemori, H., Nakatsuji, N., Yamamoto, M., Miyabayashi, T., Lutzko, C., Pera, M. F. and Kahn, M.	Wnt signaling orchestration with a small molecule DYRK inhibitor provides long-term xeno-free human pluripotent cell expansion.	Stem Cells Translational Medicine	2012;1	18–28	2012

雑誌

中畑　龍俊

発表者氏名	論文タイトル名	発表誌名	巻号	ページ	出版年
Morishima T., Watanabe K., Niwa A., Fujino H., Matsubara H., Adachi S., Suemori H., Nakahata T., Heike T.	Neutrophil differentiation from human-induced pluripotent stem cells	J. Cell. Physiol.	226	1283-1291	2011
Yamanaka Y., Kitano A., Takao K., Prasansuklab A., MushirodaT., Yamazaki K., Kumada T., Shibata M., Takaoka Y., Awaya T., Kato T., Nakahata T., Heike T.	Inactivation of fibroblast growth factor binding protein 3 causes anxiety-related behaviors	Mol. Cell. Neurosci.	46	200-212	2011
Kamio T., Ito E., Ohara A., Kosaka Y., Tsuchida M., Yagasaki H., Mugishima H., Yabe H., Morimoto A., Ohga S., Muramatsu H.,Hama A., Kaneko T., Nagasawa M., Kikuta A., Osugi Y., Bessho F., Nakahata T., Tsukimoto I., Kojima S.	Relapse of aplastic anemia in children after immunosuppressive therapy: a report from the Japan Childhood Aplastic Anemia Study Group	Haematologica	96	814-819	2011
Wakao S., Kitada M., Kuroda Y., Shigemoto T., Matsuse D., Akashi H., Tanimura Y., Tsuchiyama K.,Kikuchi T., Goda M., Nakahata T., Fujiyoshi Y., Dezawa M.	Multilineage-differentiating Stress Enduring (Muse) cells are a primary source of iPS cells in human fibroblasts.	Proc. Natl. Acad. Sci. USA	108	9875-9880	2011

Yoshida N., Yagasaki H., Hama A., Takahashi Y., Kosaka Y., Kobayashi R., Yabe H., Kaneko T., Tsuchida M., Ohara A., Nakahata T., Kojima S.	Predicting response to immunosuppressive therapy in childhood aplastic anemia	Haematologica	96	771-774	2011
Kawagoe S., Higuchi T., Xing-Li M., Shimada Y., Dhimizu H., Fukuda T., Chang H., Nakahata T., Fukada S., Ida H., Ohashi T., Eto Y.	Generation of induced pluripotent stem (iPS) cells derived from a murine model of Pompe disease and differentiation of Pompe-iPS cells into skeletal muscle cells.	Mol. Genet. Metab.	104	123-128	2011
Niwa A., Heike T., Umeda K., Oshima K., Kato I., Sakai H., Suemori H., Nakahata T., Saito M.	A novel serum-free monolayer culture for orderly hematopoietic differentiation of human pluripotent cells via mesodermal progenitors.	PLoS ONE	6	e22261	2011
Murata Y., Yasumi T., Shirakawa R., Izawa K., Sakai H., Abe J., Tanaka N., Kawai T., Oshima K., Saito M. Nishikomori R., Ohara O.、Ishii E., Nakahata T., Horiuchi H., Heike T.	Rapid diagnosis of familial hemophagocytic lymphohistiocytosis type 3 (FHL3) by flow cytometric detection of intraplatelet Munc 13-4 protein.	Blood	118	1225-1230	2011
Yahata N., Asai M., Kitaoka S., Takahashi K., Asaka I., Hioki H., Kaneko T., Maruyama K., Saido T.C., Nakahata T., Asada T., Yamanaka S., Iwata N., Inoue H.	Anti-Ab Drug Screening Platform Using Human iPS Cell-Derived Neurons for the Treatment of Alzheimer's Disease.	PLoS ONE	6	e25788	2011
Kato I, Niwa A, Heike T, Fujino H, Saito MK, Umeda K., Hiramatsu H., Ito M., Morita M., Nishinaka Y., Adachi S., Ishikawa F., Tatsutoshi Nakahata T.	Identification of Hepatic Niche Harboring Human Acute Lymphoblastic Leukemic Cells via the SDF-1/CXCR4 Axis.	PLoS ONE	6	e27042	2011

Tanaka N., Nishikomori R., Saito M., Izawa K., Sakuma M., Morimoto T., Kambe N., Watanabe S., Oshima K., Ohara O.、Goldbach-Mansky R., Aksentijevich I., Arostegui J.I., Yague Jm Joost F., van Gijn M.E., SaintBasile G., Pontillo A., Kawai T., Yasumi T., Nakahata T., Horiuchi H., Heike T.	High incidence of NLRP3 somatic mosaicism in chronic infantile neurological cutaneous and articular syndrome patients; the results of an international multicenter collaborative study.	Arthritis Rheum.	63	3625-3632	2011
Hiejima E., Komatsu H., Takeda Y., Sogo T., Inui A., Okafuji I., Nishikomori R., Nakahata T., Fujisawa T.	Acut liver failure in young children with systemic-onset juvenile idiopathic arthritis without macrophage activation syndrome: Report of two cases.	J. Pediatr. Child Health			in press
Sakai H., Okafuji I., Nishikomori R., Abe J., Izawa K., Kambe N., Yasumi T., Nakahata T., Heike T.	The CD40-CD40L axis and INF-g play critical roles in Langerhans giant cell formation.	Int. Immunol.			in press
IzawaK., Hijikata A., Tanaka N., Kawai T., Saito M.K., Goldbach-Mansky R., Aksentijevich I., Yasumi T., Nakahata T., Heike T., Nishikomori R., OharaO.	Detection of base substitution–type somatic mosaicism of the NLRP3 gene with >99.9% statistical confidence by massively parallel sequencing.	DNA Res.			in press

書籍

西田　幸二

著者氏名	論文タイトル名	書籍全体の編集者名	書籍名	出版社名	出版地	出版年	ページ
大家義則，西田幸二	組織幹細胞と角膜再生	井川洋二ら	実験医学	羊土社	東京	2011	3109-3112

雑誌

西田　幸二

発表者氏名	論文タイトル名	発表誌名	巻号	ページ	出版年
Miki Kikuchi, Ryuhei Hayashi, Sachiko Kanakubo, Ayumi Ogasawara, Masayuki Yamato, Noriko Osumi and Kohji Nishida	Neural crest-derived multipotent cells in the adult mouse iris stroma	Genes to Cells	16	273-281	2011
Miharu Sakurai, Ryuhei Hayashi,Tomofumi Kageyama, Masayuki Yamato,Kohji Nishida	Induction of putative stratified epithelial progenitor cells in vitro from mouse-induced pluripotent stem cells	J Artif Organs	14	58-66	2011
辻川元一，西田幸二	臨床応用の進歩　眼科角膜領域再生医療	日本臨床	69巻12号	2235-2240	2011
相馬剛至，西田幸二	ドナー検査と保存法	眼科	53巻12号	1709-1713	2011
相馬剛至，西田幸二	DSAEKのドナー挿入法	眼科手術	24巻4号	401-403	2011
相馬剛至，西田幸二	角結膜　培養上皮細胞シート移植	眼科	53巻10号	1451-1455	2011

桜田一洋，森山剛，西田幸二，畠賢一郎，中西淳	再生医療の産業化に対して必要な仕組みとは	再生医療	10巻2号	111-124	2011
林竜平，西田幸二	幹細胞を用いた角膜再生医療	再生医療	10巻2号	104-108	2011

IV. 研究成果の刊行物・別刷

Grafted human-induced pluripotent stem-cell–derived neurospheres promote motor functional recovery after spinal cord injury in mice

Satoshi Nori[a,b,1], Yohei Okada[a,c,1], Akimasa Yasuda[a,b], Osahiko Tsuji[b], Yuichiro Takahashi[a,b], Yoshiomi Kobayashi[a,b], Kanehiro Fujiyoshi[b], Masato Koike[d], Yasuo Uchiyama[d], Eiji Ikeda[e,f], Yoshiaki Toyama[b], Shinya Yamanaka[g], Masaya Nakamura[b,2], and Hideyuki Okano[a,2]

[a]Department of Physiology, [b]Department of Orthopaedic Surgery, [c]Kanrinmaru-Project, School of Medicine, Keio University, Shinjuku, Tokyo 160-8582, Japan; [d]Department of Cell Biology and Neuroscience, Juntendo University Graduate School of Medicine, Bunkyoku, Tokyo 113-8421, Japan; [e]Department of Pathology, School of Medicine, Keio University, Shinjuku, Tokyo 160-8582, Japan; [f]Department of Pathology, Yamaguchi University Graduate School of Medicine, Ube, Yamaguchi 755-8505, Japan; and [g]Center for iPS Cell Research and Application, Kyoto University, Shogoin, Sakyoku, Kyoto 606-8507, Japan

Edited by Fred H. Gage, The Salk Institute, San Diego, CA, and approved September 1, 2011 (received for review May 20, 2011)

Once their safety is confirmed, human-induced pluripotent stem cells (hiPSCs), which do not entail ethical concerns, may become a preferred cell source for regenerative medicine. Here, we investigated the therapeutic potential of transplanting hiPSC-derived neurospheres (hiPSC-NSs) into nonobese diabetic (NOD)-severe combined immunodeficient (SCID) mice to treat spinal cord injury (SCI). For this, we used a hiPSC clone (201B7), established by transducing four reprogramming factors (Oct3/4, Sox2, Klf4, and c-Myc) into adult human fibroblasts. Grafted hiPSC-NSs survived, migrated, and differentiated into the three major neural lineages (neurons, astrocytes, and oligodendrocytes) within the injured spinal cord. They showed both cell-autonomous and noncell-autonomous (trophic) effects, including synapse formation between hiPSC-NS–derived neurons and host mouse neurons, expression of neurotrophic factors, angiogenesis, axonal regrowth, and increased amounts of myelin in the injured area. These positive effects resulted in significantly better functional recovery compared with vehicle-treated control animals, and the recovery persisted through the end of the observation period, 112 d post-SCI. No tumor formation was observed in the hiPSC-NS–grafted mice. These findings suggest that hiPSCs give rise to neural stem/progenitor cells that support improved function post-SCI and are a promising cell source for its treatment.

stem-cell–based medicine | cell transplantation | neurotrauma | synaptic connection

Stem-cell–based approaches, such as the transplantation of neural stem/progenitor cells (NS/PCs), are promising sources of therapies for various central nervous system disorders (1–3). Previous studies reported functional recovery after transplantation of NS/PCs into the injured spinal cord of rodents and nonhuman primates (4–9). Furthermore, recent studies revealed that embryonic stem cells (ESCs) can generate neural cells including NS/PCs (10–12) and oligodendrocyte precursor cells (OPCs) (13, 14). Therefore, human ESC-based therapies are moving out of the laboratory and into clinical treatments for spinal cord injury (SCI) (12, 13, 15). However, the use of human ESC-based therapies is complicated by ethical concerns in certain countries. To avoid the problems associated with ESCs, we previously established induced pluripotent stem cells (iPSCs) from mouse fibroblasts (16, 17) and confirmed the therapeutic potential of iPSC-derived neurospheres (iPSC-NSs) for treating SCI in animal models (18).

Here, aiming at human iPSC-based therapies for SCI patients, we examined the therapeutic potential of human iPSC-NSs by transplanting them into nonobese diabetic severe combined immunodeficient (NOD-SCID) SCI model mice. We used a clone from human iPSCs (hiPSCs) that we established from adult human dermal fibroblasts by the retroviral transduction of four reprogramming factors; for the clone used in this study, 201B7, the factors were Oct3/4, Sox2, Klf4, and c-Myc (19). These grafted hiPSC-NSs survived, migrated, and differentiated into the three neural lineages in the injured spinal cord. They promoted angiogenesis and axonal regrowth and preserved myelination, and some formed synapses with host mouse neurons. These positive effects promoted functional recovery that persisted for up to 112 d after SCI, without tumor formation.

These findings indicated that neurospheres derived from hiPSCs are a potential cell source for transplantation therapy for SCI.

Results

Grafted hiPSC-NSs Survived, Migrated, and Differentiated into Three Neural Lineages. Contusive SCI was induced at the Th10 level in NOD-SCID mice, and 5×10^5 Venus$^+$ hiPSC-NSs or PBS was injected into the lesion epicenter, 9 d after injury. To examine the effects of grafted hiPSC-NSs in the injured spinal cord, histological analyses were performed 56 d after SCI [after functional recovery, based on the Basso mouse scale (BMS) score, was observed to plateau]. Ten mice in each group were killed on day 56, and 18 mice grafted with hiPSC-NSs and 16 PBS-injected mice remained. These mice were assessed by BMS and for long-term safety of the grafted hiPSC-NSs, 112 d after SCI (Table S1).

On day 56, the grafted hiPSC-NSs had survived and migrated into the host spinal cord (Fig. 1 *A* and *B*). To examine their differentiation potentials, we performed immunohistochemical analyses and quantified the proportion of Venus$^+$ cells immunopositive for cell-type–specific markers. The engrafted hiPSC-NSs differentiated into neuronal nuclei (NeuN)$^+$ and β-tubulin isotype III (βIII tubulin)$^+$ neurons, glial fibrillary acidic protein (GFAP)$^+$ astrocytes, and adenomatous polyposis coli CC-1 (APC)$^+$ oligodendrocytes (Fig. 1 *C*–*F*). The βIII tubulin$^+$/Venus$^+$ neurons comprised 49.1 ± 2.0% of the Venus$^+$ cells, and the mature NeuN$^+$/Venus$^+$ neurons comprised 22.9 ± 1.0%. Thus, 56 d after SCI, about 50% of the grafted hiPSC-NSs had differentiated into neurons, about half of which were mature neurons. GFAP$^+$/Venus$^+$ astrocytes comprised 17.0 ± 1.2%, but APC$^+$/Venus$^+$ oligodendrocytes were rare (3.0 ± 0.4%). Nestin$^+$/Venus$^+$ NS/PCs made up 10.7 ± 2.2% of the total (Fig. 1*G*).

Author contributions: Y.U., Y. Toyama, S.Y., M.N., and H.O. designed research; S.N., Y.O., A.Y., O.T., Y. Takahashi, Y.K., K.F., M.K., and E.I. performed research; S.N., M.K., and E.I. analyzed data; and S.N., Y.O., M.K., M.N., and H.O. wrote the paper.

The authors declare no conflict of interest.

This article is a PNAS Direct Submission.

Freely available online through the PNAS open access option.

[1]S.N. and Y.O. contributed equally to this work.

[2]To whom correspondence may be addressed. E-mail: hidokano@a2.keio.jp or masa@sc.itc.keio.ac.jp.

This article contains supporting information online at www.pnas.org/lookup/suppl/doi:10.1073/pnas.1108077108/-/DCSupplemental.

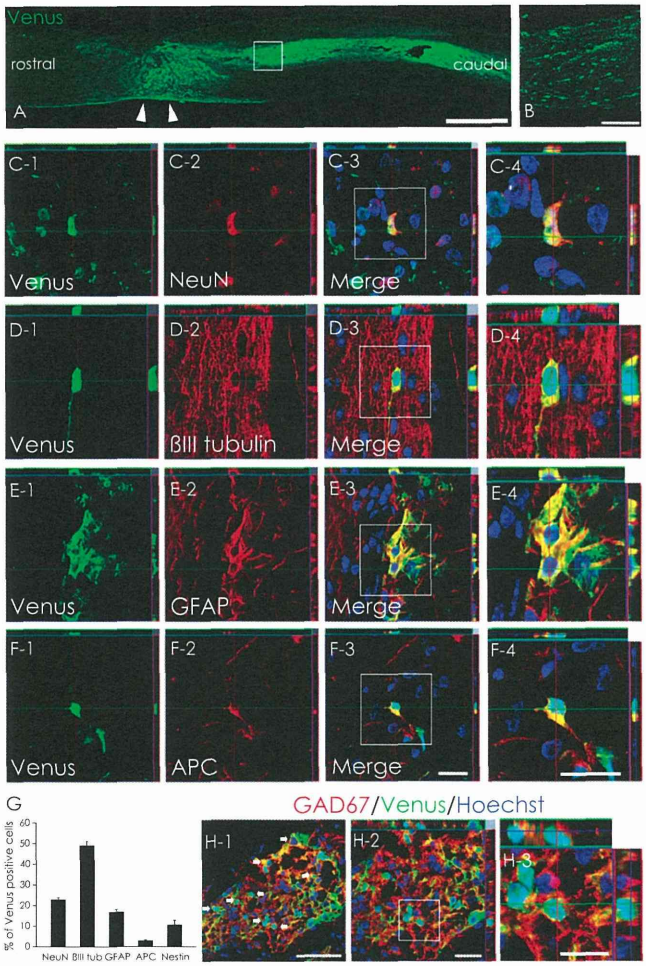

Fig. 1. In vivo differentiation of hiPSC-NSs. (*A* and *B*) Venus$^+$ hiPSC-NSs were integrated at or near the lesion epicenter (arrowheads). (Scale bars, 1000 μm in *A*; 100 μm in *B*.) (*C–F*) Representative images of Venus$^+$-grafted cells labeled with the neural markers NeuN$^+$ (mature neurons) (*C*); βIII tubulin$^+$ (all neurons) (*D*); GFAP$^+$ astrocytes (*E*); and APC$^+$ oligodendrocytes (*F*). (Scale bar, 20 μm.) (*G*) Percentages of cell-type–specific marker-positive cells among the Venus$^+$-grafted cells 56 d after SCI. Values are means ± SEM ($n = 4$). (*H*) Most hiPSC-derived neurons differentiated into GAD67$^+$ (GABAergic) neurons. (Scale bars, 50 μm in *H-1*; 20 μm in *H-2*; and 10 μm in *H-3*.)

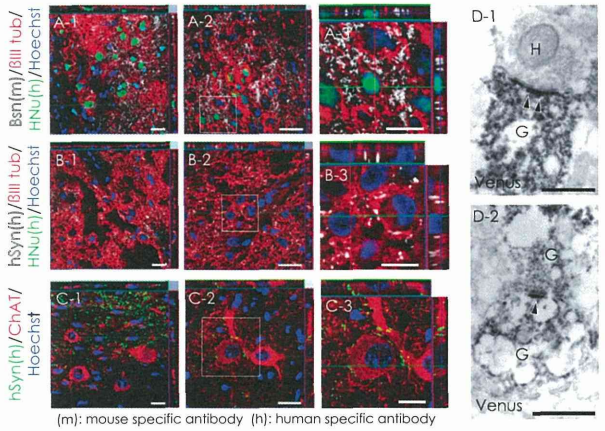

Fig. 2. Evidence for synapse formation between hiPSC-derived neurons and host mouse spinal cord neurons. (*A*) Sections were triple-stained with HNu (green), βIII tubulin (red), and the presynaptic marker Bassoon (Bsn, white). The Bsn antibody used here recognized the rat and mouse, but not human, protein. (*B*) Sections triple-stained for HNu (green), βIII tubulin (red), and the human-specific presynaptic marker hSyn (white). (*C*) Confocal images showing a large number of somatic and dendritic terminals from graft-derived nerve cells on host motor neurons at the ventral horns. (*D*) Electron microscopy showing synapse formation between host mouse neurons and graft-derived Venus$^+$ (black) human neurons: the pre- and postsynaptic structures indicated transmission from a host neuron to a graft-derived neuron (*D-1*) and from a graft-derived neuron to a graft-derived neuron (*D-2*). H, host neuron; G, graft-derived neuron; arrowheads, postsynaptic density. (Scale bars, 20 μm in *A-1*, *A-2*, *B-1*, *B-2*, *C-1*, and *C-2*; 10 μm in *A-3*, *B-3*, and *C-3*; and 0.5 μm in *D*.)

Because 22.9% of the hiPSC-NSs differentiated into mature neurons, we next examined their neurotransmitter phenotype, using neurotransmitter-specific markers. Of the Venus$^+$ cells, 15.8 ± 2% were glutamic acid decarboxylase 67 (GAD67)$^+$, indicating that 69% (15.8/22.9% = 69.0%) of the hiPSC-NS–derived mature neurons were GABAergic (Fig. 1*H*). We also found small numbers of Venus$^+$ tyrosine hydroxylase (TH)$^+$ neurons and choline acetyltransferase (ChAT)$^+$ cholinergic neurons (Fig. S1 *A* and *B*).

Synapse Formation Between hiPSC-Derived Neurons and Host Mouse Neurons. To evaluate the ability of the hiPSC-NS–derived neurons to integrate with the host neural circuitry, triple immunostaining was performed with antibodies to human nuclear protein (HNu), βIII tubulin, and the presynaptic protein Bassoon (Bsn). The anti-Bsn antibody is a monoclonal that selectively recognizes mouse and rat, but not human epitopes. Grafted βIII tubulin$^+$/HNu$^+$ cells in the neural parenchyma were observed in contact with the synaptic boutons of host neurons (Fig. 2*A*). In addition, triple immunostaining for HNu, βIII tubulin, and human-specific synaptophysin (hSyn) revealed dense fields of boutons apposed to βIII tubulin$^+$/HNu$^-$ host mouse neurons (Fig. 2*B*). These host neurons in the ventral gray matter were ChAT$^+$, and some of the boutons represented graft-specific terminals (Fig. 2*C*). Immunoelectron microscopy revealed Venus$^+$ (i.e., human) presynaptic and postsynaptic structures and synapses between host mouse neurons and Venus$^+$ hiPSC-derived neurons at the injured site (Fig. 2*D*).

Transplantation of hiPSC-NSs Enhanced Angiogenesis and Axonal Regrowth but Did Not Induce Abnormal Innervation of Pain-Related CGRP$^+$ Afferents After SCI. To evaluate the effects of hiPSC-NS transplantation on angiogenesis after SCI, immunohistochemical analyses for platelet endothelial cell adhesion molecule-1 (PECAM-1) were performed. There were significantly more PECAM-1$^+$ blood vessels at the lesion epicenter in the hiPSC-NS group than in the control group (Fig. 3 *A–C*). To determine the source of the angiogenic signals, we examined the vascular endothelial growth factor (VEGF) expression in the grafted spinal cord by immunohistochemistry (Fig. 3*D*). Quantitative analyses revealed that the VEGF$^+$ area at the lesion epicenter was significantly larger in the hiPSC-NS group than in the control group (Fig. 3*E*). Furthermore, both GFAP$^+$/Venus$^+$ hiPSC-derived astrocytes (Fig. 3*F*) and GFAP$^+$/Venus$^-$ host mouse astrocytes expressed VEGF (Fig. 3*G*), consistent with the results of RT-PCR (Fig. 3 *H* and *I*). Note that the mouse *Vegf* mRNA expression level was higher in the hiPSC-NS–grafted mice than in PBS-injected mice.

Because angiogenesis generally improves tissue sparing, we examined the atrophic changes of the injured spinal cord by hematoxylin–eosin (H&E) staining. Unlike the hiPSC-NS group, atrophic changes of the injured spinal cord were prominent in the control group (Fig. 3 *J* and *K*). Quantitative analysis revealed significant differences in the transverse area of the spinal cord between the control and hiPSC-NS group, suggesting that the hiPSC-NS transplantation prevented atrophy of the injured spinal cord (Fig. 3*L*). Luxol fast blue (LFB) staining also revealed

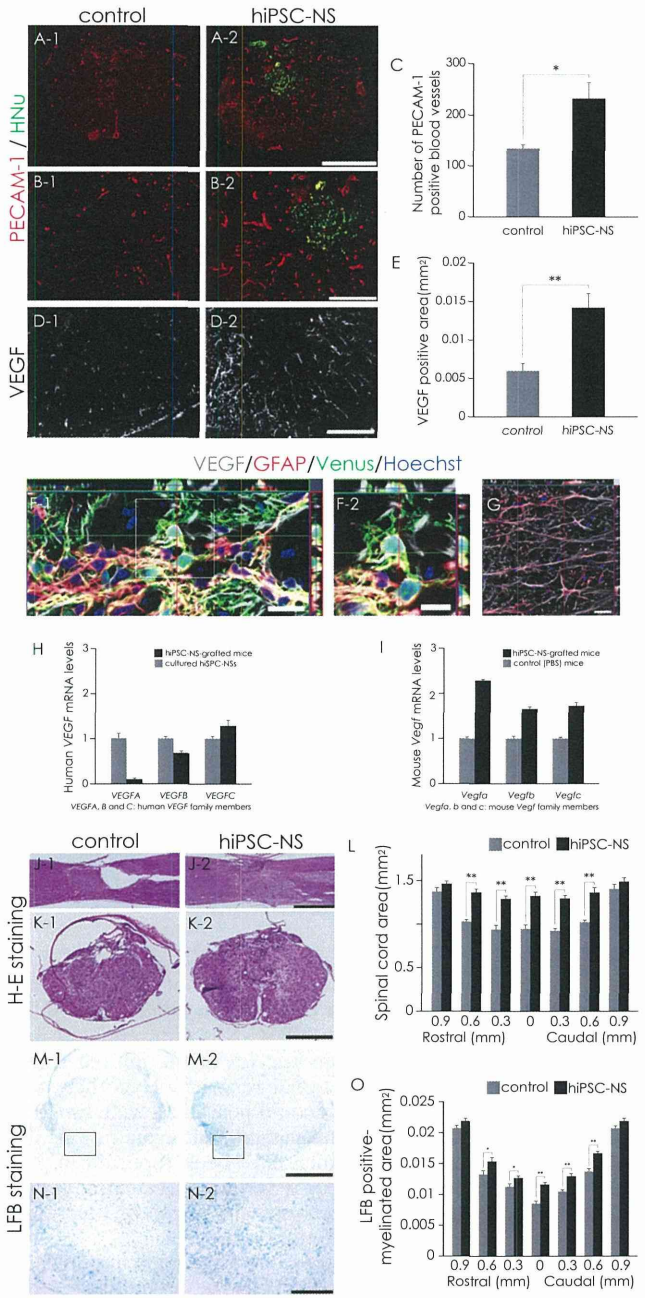

Fig. 3. Transplanted hiPSC-NSs enhanced angiogenesis and prevented atrophic changes and demyelination after SCI. (*A* and *B*) Representative images of PECAM-1$^+$ blood vessels. (*C*) Quantitative analysis of PECAM-1$^+$ blood vessels at the lesion epicenter. Values are means ± SEM (n = 4). (*D*) Representative images of axial sections stained for VEGF. (*E*) Quantitative analysis of the VEGF$^+$ area at the lesion epicenter. Values are means ± SEM (n = 4). (*F* and *G*) Expression of VEGF in GFAP$^+$ astrocytes among Venus$^+$-graft–derived human cells (yellow indicates VEGF$^+$, GFAP$^+$, and Venus$^+$ cells) (*F*) and host mouse-derived cells (*G*) in the spinal cord. (*H*) Expression of human *VEGF* mRNA (*VEGFA*, *-B*, and *-C* are the human *VEGF* family members) 5 d after the hiPSC-NSs were transplanted (black bars) compared with cultured hiPSC-NSs before transplantation (gray bars). Values are means ± SEM (n = 3, each). Human *VEGF* expression was undetectable in the spinal cord of mice treated with PBS. (*I*) Expression of mouse *Vegf* mRNA (*Vegfa*, *-b*, and *-c* are the mouse *Vegf* family members) 5 d after hiPSC-NS transplantation (black bars) or PBS injection (gray bars) into the spinal cord. The mouse *Vegf* expression level was higher in the hiPSC-NS–grafted mice than in PBS-injected mice. Values are means ± SEM (n = 3, each). (*J* and *K*) Representative H&E-stained images of sagittal and axial sections at the lesion epicenter 56 d after SCI. (*L*) Quantitative analysis of the spinal cord area measured in H&E-stained axial sections at different regions. Values are means ± SEM (n = 6). (*M* and *N*) Representative LFB-stained images of the axial sections at the lesion epicenter 56 d after SCI. (*O*) Quantitative analysis of the myelinated area by LFB-stained axial sections at different regions. Values are means ± SEM (n = 6). *P < 0.05, **P < 0.01. (Scale bars, 500 μm in *A*, *K*, and *M*; 200 μm in *B*; 100 μm in *D* and *N*; 20 μm in *F-1* and *G*; 10 μm in *F-2*; and 1,000 μm in *J*.)

a greater preservation of myelinated areas in the hiPSC-NS group compared with the control group (Fig. 3 *M–O*).

To evaluate the effects of hiPSC-NS transplantation on axonal regrowth after SCI, we examined the expression of neurofilament 200 kDa (NF-H), 5-hydroxytrytamine (5HT), and growth-associated protein 43 (GAP43) in the injured spinal cord by immunohistochemistry. There were significantly more NF-H$^+$ neuronal fibers in the hiPSC-NS group than in the control group (Fig. 4 *A* and *B*). 5HT$^+$ fibers, descending serotonergic raphespinal tract axons that are important for the motor functional recovery of hind limbs (20–22), were observed at the lumbar intumescence in all mice (Fig. 4*C*). Contusive SCI resulted in a significant decrease in the number of 5HT$^+$ fibers. Relative to mice at 7 d after SCI (2 d before the transplantation), by 56 d after SCI a slight but significant increase in the 5HT$^+$ fiber area was seen in the control group, and the hiPSC-NS group showed an even greater enhancement (Fig. 4 *C* and *D*).

GAP43$^+$ axons, which are regrowing (23), were detected in the distal cords of all mice, but in the hiPSC-NS group, there were significantly more GAP43$^+$ fibers in the ventral region 1 mm caudal to the lesion epicenter (Fig. 4 *E* and *F*), suggesting that the hiPSC-NS transplantation promoted axonal regrowth in the injured spinal cord. We also observed hiPSC-NS–derived astrocytes closely associated with NF-H$^+$ fibers and 5HT$^+$ fibers (Fig. 4 *G* and *H*). Moreover, RT-PCR revealed the expression of neurotrophic factors (NGF, BDNF, and hepatocyte growth factor, HGF), which are associated with the axonal growth and survival of existing neurons, by both the grafted human cells and the host mouse tissues (Fig. 4 *I* and *J*).

To examine the effect of hiPSC-NSs on structural changes in pain afferents entering the dorsal horn of the spinal cord above and below the injured spinal segments, we investigated the distribution of calcitonin gene-related peptide (CGRP$^+$) fibers, which are involved in peripheral and spinal pain mechanisms (6, 24, 25). We quantified the areas of CGRP$^+$ fibers in lamina III, 4 mm rostral and 4 mm caudal to the lesion epicenter. There were no significant differences in the areas of CGRP$^+$ fibers in lamina III between the hiPSC-NS and control groups (Fig. S2 *A–C*).

Transplanted hiPSC-NSs Promoted Motor Functional and Electrophysiological Recovery After SCI. We evaluated the motor functional recovery by BMS score, Rotarod test, and the DigiGait system. The BMS score showed significantly better functional recovery in the hiPSC-NS than the control group 21 d after SCI and thereafter (Fig. 5*A*). In the Rotarod test, the hiPSC-NS group showed a significantly longer running time than the control group 56 d post-SCI (Fig. 5*B*). The DigiGait system measures the treadmill gait, as an objective evaluation of motor function (26, 27). Whereas all of the hiPSC-NS–grafted mice (n = 18) could walk on the treadmill at 8 cm/s, a subset of the control mice (4 out of 16) could not maintain this speed. The profile of stride length at 8 cm/s clearly demonstrated a significantly better recovery of motor function in the hiPSC-NS–grafted mice compared with the 12 control mice that could walk at this speed (Fig. 5*C*).

Motor-evoked potential (MEP) was used to measure the functional recovery in all of the mice electrophysiologically. The latency of the motor-evoked potential was also measured, from the onset of stimulus to the first response of each wave. At 112 d after SCI, waves were detected in most of the hiPSC-NS group (14 of 17 mice), but none were detected in the control group (0 of 15 mice) (Fig. 5*D*). The average signal-to-response latency in the hiPSC-NS group was 4.6 ± 0.1 ms. Consistent with the

NEUROSCIENCE

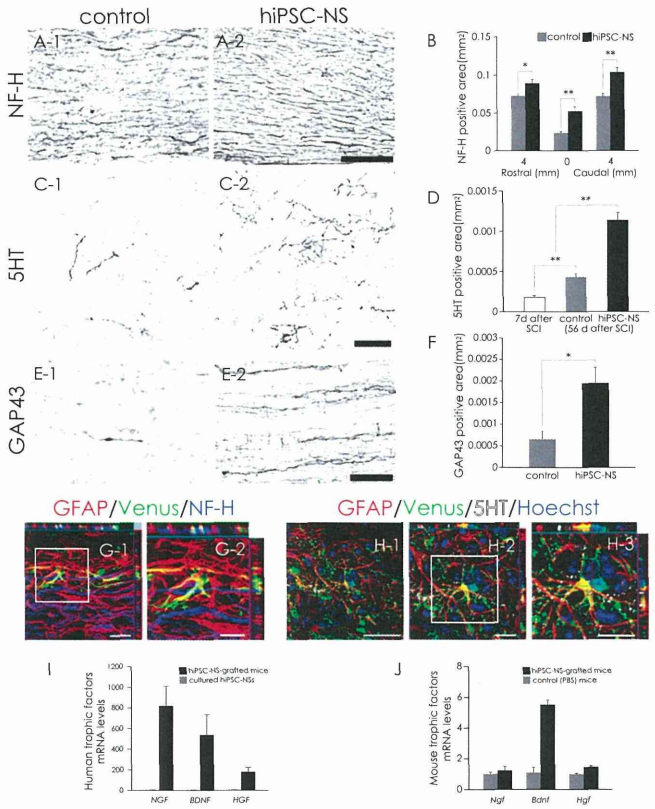

Fig. 4. Transplanted hiPSC-NSs enhanced axonal growth after SCI. (*A*) Representative images of sagittal sections stained for NF-H at the lesion epicenter. (*B*) Quantitative analysis of the NF-H$^+$ area. Values are means ± SEM (n = 4). (*C*) Representative images of axial sections stained for 5HT at the lumbar intumescence. (*D*) Quantitative analysis of the 5HT$^+$ area at the lumbar intumescence in axial sections. Values are means ± SEM (n = 6 each in the 7 d and control 56 d after SCI groups, and n = 5 in the hiPSC-NS (56 d after SCI) group). (*E*) Representative images of midsagittal sections stained for GAP43 in the ventral region 1 mm caudal to the lesion epicenter. (*F*) Quantitative analysis of the GAP43$^+$ area in midsagittal sections. Values are means ± SEM (n = 4). (*G* and *H*) NF-H$^+$ neural fibers and 5HT$^+$ (serotonergic) fibers extended in association with GFAP$^+$/Venus$^+$-graft–derived human astrocytes. (*I*) Expression of human neurotrophic factor mRNAs (*NGF*, *BDNF*, and *HGF*) 5 d after hiPSC-NS transplantation (black bars) compared with cultured hiPSC-NSs before transplantation (gray bars). Values are means ± SEM (n = 3, each). (*J*) Expression of mouse neurotrophic factor mRNAs (*Ngf*, *Bdnf*, and *Hgf*) 5 d after hiPSC-NS transplantation (black bars) or PBS injection (gray bars) into the spinal cord. Values are means ± SEM (n = 3, each). *P < 0.05, **P < 0.01. (Scale bars, 100 μm in *A*; 50 μm in *C*, *E*, and *H-1*; 20 μm in *G-1*, *H-2*, and *H-3*; and 10 μm in *G-2*.)

electrophysiology results, α-CaM kinase 2$^+$ descending motor axons were observed to persist in the lesion epicenter in the hiPSC-NS group (Fig. S3).

Long-Term Observation Revealed No Tumor Formation After hiPSC-NS Transplantation. To investigate the long-term safety of the grafted hiPSC-NSs, we extended the follow-up period to 112 d after SCI. Motor functional recovery was maintained in the hiPSC-NS group for the entire period (Fig. 6*A*), the hiPSC-NS–grafted mice showed no tumor formation (Fig. 6*B*), and the grafted cells exhibited normal neural differentiation (Fig. 6*C*). We determined the proportion of Venus$^+$ grafted cells that were immunopositive for each cell-type–specific marker 112 d after SCI. The grafted hiPSC-NSs had differentiated into NeuN$^+$ (40.2 ± 2.8%), βIII tubulin$^+$ (50.7 ± 2.0%), GFAP$^+$ (18.1 ± 2.2%), APC$^+$ (8.9 ± 1.6%), and Nestin$^+$ (7.5 ± 1.0%) cells. For comparison, at 56 d after SCI, the grafted cells had differentiated

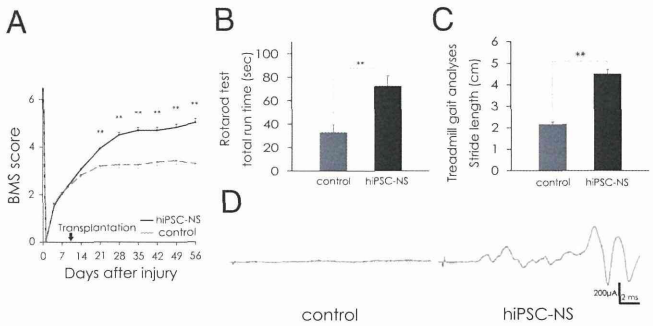

Fig. 5. Transplanted hiPSC-NSs promoted motor functional and electrophysiological recovery after SCI. (*A*) Motor function in the hindlimbs was assessed weekly by the BMS score for 56 d. Values are means ± SEM. (*B*) Rotarod test 56 d after SCI. Graph shows the total run time. Values are means ± SEM. (*C*) Treadmill gait analysis using the DigiGait system 56 d after SCI. Graph shows stride length. Values are means ± SEM. (*D*) Electrophysiological analysis performed 112 d after SCI. MEP waves were detected in most of the hiPSC-NS group (14 out of 17), whereas they were not detected in the control group (0 out of 15). **P < 0.01. Behavioral analyses were assessed by two observers who were blind to the treatment.

into NeuN$^+$ (22.9 ± 1.0%), βIII tubulin$^+$ (49.1 ± 2.0%), GFAP$^+$ (17.0 ± 1.2%), APC$^+$ (3.0 ± 0.4%), and Nestin$^+$ (10.7 ± 2.2%) cells (Fig. 6*D*). Notably, significantly higher percentages of NeuN$^+$ mature neurons and APC$^+$ oligodendrocytes were present at 112 d than at 56 d after SCI, whereas the percentage of graft-derived human Nestin$^+$ NS/PCs slightly decreased. We also examined the amount of proliferation among the grafted cells by K_i-67 labeling. The percentage of K_i-67$^+$/HNu$^+$ cells was significantly decreased between 56 d post-SCI (1.1 ± 0.2%) and 112 d post-SCI (0.7 ± 0.1%). The K_i-67$^+$/HNu$^+$ cells were dispersed throughout the graft area without evidence of clustering at particular sites.

Discussion

In the present study, we used clone 201B7 of hiPSC-derived neurospheres as a cell source to treat SCI in adult NOD-SCID mice. We demonstrated that the hiPSC-NSs differentiated into neurons, astrocytes, and oligodendrocytes in the injured spinal cord and promoted motor functional recovery. Hypothetically, the transplantation of hiPSC-NSs could result in a wide range of positive effects, including angiogenesis, axonal regeneration, and local-circuitry reconstruction, which have been reported in previous studies using rodent ESCs or iPSCs for SCI treatment (12, 18). All these mechanisms could contribute to motor functional recovery after hiPSC-NS transplantation for SCI.

Angiogenesis after SCI promotes endogenous repair and supports axonal outgrowth (28, 29). Here we observed that the transplantation of hiPSC-NSs enhanced angiogenesis and tissue sparing after SCI. Astrocytes express angiogenic growth factors such as VEGF under hypoxic conditions (12, 30, 31), and we observed that the hiPSC-derived astrocytes and host astrocytes expressed VEGF, suggesting that the transplantation of hiPSC-NSs promoted VEGF expression in both host- and graft-derived astrocytes.

Motor functional recovery was also supported by the axonal regrowth that was promoted by the transplanted hiPSC-NSs. Our immunohistochemical analyses revealed grafted hiPSC-derived GFAP$^+$ astrocytes closely associated with NF-H$^+$ and 5HT$^+$ fibers. Graft-derived astrocytes are reported to promote the regrowth of NF-H$^+$ and 5HT$^+$ fibers by offering a growth-permissive substrate (12, 18, 32). Furthermore, neurotrophic factors such as NGF, BDNF, and HGF play critical roles in axonal growth and in the survival of existing neurons (33–38). Consistent with these reports, we observed that hiPSC-NS transplantation promoted axonal regrowth at the distal spinal cord. Because our treatment induced axonal regrowth, we also exam-

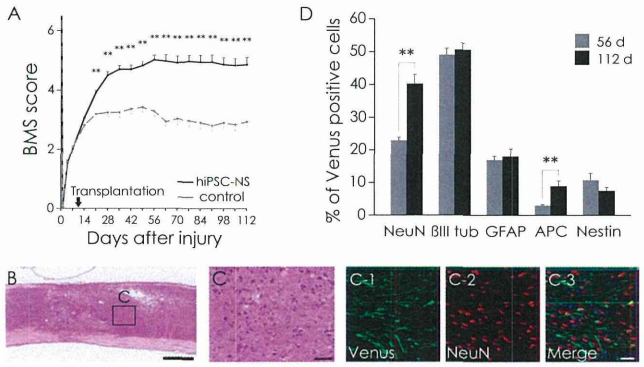

Fig. 6. Long-term observation revealed no tumor formation after hiPSC-NS transplantation. (*A*) For 112 d, motor function in the hindlimbs was assessed weekly by the BMS score. Values are means ± SEM. (*B*) Representative H&E image of hiPSC-NS–grafted mice. (*C*) Boxed area in *B*. (*C-1–C-3*) Immunohistochemistry showing normal neural differentiation of the grafted cells. (*D*) Percentages of cell-type–specific marker-positive cells among the Venus$^+$ human cells 56 and 112 d after SCI. Values are means ± SEM (n = 4 and 5, respectively). $^{**}P < 0.01$. (Scale bars, 500 μm in *B*; and 50 μm in *C*.)

ined the pain afferents entering lamina III of the spinal cord, which is closely associated with NS/PC-transplantation–induced allodynia (6). Our analysis revealed no significant differences between the hiPSC-NS and control groups. Thus, although allodynia was not assessed, our morphological data suggested that hiPSC-NS transplantation did not induce abnormal innervation by pain afferents, in contrast to a previous study in which NS/PCs derived from adult rat spinal cord were transplanted into a rat SCI model (6).

The motor functional recovery observed in this study may also be due to the formation of synapses between hiPSC-derived neurons and host mouse spinal cord neurons. Our present data support the potential for grafted hiPSC-NSs to form synapses with host neurons in the injured spinal cord. Previous studies have shown post-SCI functional improvements associated with intraspinal grafts containing neuronal progenitors either alone or in combination with other cells or interventions (4, 7, 39–43). Such studies also report that graft-derived human neurons can receive projections from host mouse neurons and that their extended processes make synapses with host neurons (39). It is likely that local neurons in the lesioned area (a mixture of preserved host neurons and graft-derived neurons) transmit signals by relay.

We observed that most of the hiPSC-derived mature neurons were GABAergic, a neurotransmitter type that plays important roles in the spinal cord by controlling the levels of motoneuronal output and sensory input, by modulating primary afferent transmitter release, and by direct postsynaptic inhibition of motoneurons (44, 45). Furthermore, hypofunctioning spinal GABAergic inhibition is involved in pathological pain states that develop due to SCI (46). Thus, synapse formation by donor-derived GABAergic neurons might be important for motor coordination within the spinal neuronal network and for the suppression of SCI-induced spasticity (8, 47) and pain (46).

The greatest potential drawback of hiPSC-based therapies is their potential for tumorigenicity. Therefore, we observed the treated animals for an extended period. Not only was functional recovery maintained in the hiPSC-NS group for 112 d after SCI, but no tumor formation occurred at all. Quantitative analysis of the phenotype of the grafted hiPSC-NSs revealed an increase in the percentages of NeuN$^+$ mature neurons and APC$^+$ oligodendrocytes at 112 d compared with 56 d after SCI, showing that most of the grafted hiPSC-NSs successfully differentiated into mature neural cells over time. Some Nestin$^+$/HNu$^+$ cells and K_i-67$^+$/HNu$^+$ cells were still present at 112 d post-SCI, although their proportions were lower than at 56 d after SCI, indicating that some grafted cells remained as NS/PCs. However, no evidence of excessive proliferation, clusters of proliferating cells, or other signs of tumor formation were observed in any of the transplant-receiving mice. Collectively, the lack of tumors, increase in NeuN numbers over time, and low Nestin and K_i-67 numbers support the possibility that this approach will be safe in humans.

Consistent with our findings, previous studies using human fetal NS/PCs showed some Nestin$^+$/HNu$^+$ cells that were negative for the proliferative markers K_i-67 and proliferating cell nuclear antigen in the striatum of NOD-SCID mice, 6 mo after transplantation (48), 28–34% Nestin$^+$/HNu$^+$, and 2–4% K_i-67$^+$/HNu$^+$ cells were in the spinal cord of NOD-SCID mice 4 mo after transplantation (5), and 11–14% Nestin$^+$/HNu$^+$ and 3–5% K_i-67$^+$/HNu$^+$ cells were in the spinal cord of nude rats 6 mo after transplantation (49). Notably, no tumor formation was observed in any of these studies, despite the presence of Nestin$^+$- and K_i-67$^+$–grafted cells, even after long-term observation.

Recently, clinical trials of human stem-cell–based therapy for SCI have been launched, using human NS/PCs (4, 5) or human ESC-derived OPCs (15). In this paradigm, OPC-mediated restoration of myelination and trophic effects are the most likely mechanisms for the resulting benefits. Besides overcoming concerns about immune responses and the ethics of using human ESCs (hESCs), our present study suggests that grafted hiPSC-NSs might be more beneficial than hESCs, because the hiPSC-NSs gave rise to GABAergic neurons, which can help to suppress SCI-induced spasticity and pain (8, 46, 47). In addition, we found that hiPSC-NSs differentiated into astrocytes and oligodendrocytes, which can exert positive effects through both cell-autonomous and noncell-autonomous (trophic) mechanisms. Nevertheless, our present results are only a first step toward clinical applications. In our future studies, the safety and effectiveness of hiPSC-derived NS/PCs will be more intensively investigated, for example, using nonhuman primate SCI models (8). In particular, hiPSCs established by delivering the reprogramming factors using a different method, such as an integration-free virus system (50), or a virus-free (51) or transgene-free system (52–54), or by using (HLA)-homozygous donor-derived cells (55), should be evaluated.

Materials and Methods

Cell Culture, Neural Induction, and Lentivirus Transduction. The cell culture and neural induction of hiPSCs (201B7) were performed as described previously (11, 18, 56) with slight modifications.

Lentivirus was prepared and transduced into neurospheres as described previously (11). Briefly, hiPSC-derived primary neurospheres were dissociated and infected with lentivirus expressing Venus fluorescent protein under control of the EF promoter (pCSII-EF–Venus). These primary neurospheres were passaged into secondary and tertiary neurospheres and used for transplantation.

Spinal Cord Injury Model and Transplantation. Adult female NOD-SCID mice (20–22 g) were anesthetized via an i.p. injection of ketamine (100 mg/kg) and xylazine (10 mg/kg). Contusive SCI was induced at the Th10 level using an IH impactor (60 kdyn; Precision Systems and Instrumentation), as described previously (57).

Nine days after the injury, 5×10^5 hiPSC-NSs were transplanted into the lesion epicenter of each mouse (n = 31) using a glass micropipette and stereotaxic injector (KDS310; Muromachi-Kikai). An equal volume of PBS was injected instead into control mice (n = 29).

Behavioral and Histological Analyses. Behavioral analyses were evaluated using the BMS, Rotarod apparatus (Muromachi Kikai), and the DigiGait system (Mouse Specifics) (detailed protocols are described in *SI Materials and Methods*). For histological analyses, mice were deeply anesthetized and intracardially perfused with 4% paraformaldehyde (PFA; pH 7.4). The dissected spinal cords were then sectioned into axial/sagittal sections using a cryostat (detailed conditions are in *SI Materials and Methods*). All behavioral and histological analyses were conducted by observers blind to the treatment. All animal experiments were approved by the ethics committee

of Keio University and were in accordance with the Guide for the Care and Use of Laboratory Animals (National Institutes of Health, Bethesda, MD).

ACKNOWLEDGMENTS. We thank Drs. K. Kitamura, N. Nagoshi, M. Mukaino, A. Iwanami, F. Renault-Mihara, S. Shibata, H. Shimada, T. Harada, S. Miyao, and H.J. Okano for technical assistance and scientific discussions; S. Kaneko for critical proofreading of the manuscript; and all the members of the H.O. and S.Y. laboratories for encouragement and generous support. We also thank Dr. K. Takahashi for the undifferentiated iPS cells. This work was supported by grants from Grants-in-Aid for Scientific Research from Japan Society for the Promotion of Science (SPS) and the Ministry of Education, Culture, Sports, Science, and Technology of Japan (MEXT); the Project for Realization of Regenerative Medicine; and Support for Core Institutes for iPS Cell Research from the MEXT; Japan Science and Technology–California Institute for Regenerative Medicine collaborative program; the Kanrinmaru project from Keio University; Research Fellowships for Young Scientists from JSPS; Keio Gijuku Academic Development Funds; by a Grant-in-Aid for the Global COE program from MEXT to Keio University; and by a Grant-in-Aid for Scientific Research on Innovative Areas (Comprehensive Brain Science Network) from the Ministry of Education, Science, Sports and Culture of Japan.

1. Björklund A, Lindvall O (2000) Cell replacement therapies for central nervous system disorders. *Nat Neurosci* 3:537–544.
2. Gage FH (2000) Mammalian neural stem cells. *Science* 287:1433–1438.
3. Lindvall O, Kokaia Z (2006) Stem cells for the treatment of neurological disorders. *Nature* 441:1094–1096.
4. Cummings BJ, et al. (2005) Human neural stem cells differentiate and promote locomotor recovery in spinal cord-injured mice. *Proc Natl Acad Sci USA* 102: 14069–14074.
5. Salazar DL, Uchida N, Hamers FP, Cummings BJ, Anderson AJ (2010) Human neural stem cells differentiate and promote locomotor recovery in an early chronic spinal cord injury NOD-scid mouse model. *PLoS ONE* 5:e12272.
6. Hofstetter CP, et al. (2005) Allodynia limits the usefulness of intraspinal neural stem cell grafts; directed differentiation improves outcome. *Nat Neurosci* 8:346–353.
7. Ogawa Y, et al. (2002) Transplantation of in vitro-expanded fetal neural progenitor cells results in neurogenesis and functional recovery after spinal cord contusion injury in adult rats. *J Neurosci Res* 69:925–933.
8. Iwanami A, et al. (2005) Transplantation of human neural stem cells for spinal cord injury in primates. *J Neurosci Res* 80:182–190.
9. Okada S, et al. (2005) In vivo imaging of engrafted neural stem cells: Its application in evaluating the optimal timing of transplantation for spinal cord injury. *FASEB J* 19: 1839–1841.
10. Okada Y, Shimazaki T, Sobue G, Okano H (2004) Retinoic-acid-concentration-dependent acquisition of neural cell identity during in vitro differentiation of mouse embryonic stem cells. *Dev Biol* 275:124–142.
11. Okada Y, et al. (2008) Spatiotemporal recapitulation of central nervous system development by murine embryonic stem cell-derived neural stem/progenitor cells. *Stem Cells* 26:3086–3098.
12. Kumagai G, et al. (2009) Roles of ES cell-derived gliogenic neural stem/progenitor cells in functional recovery after spinal cord injury. *PLoS ONE* 4:e7706.
13. Keirstead HS, et al. (2005) Human embryonic stem cell-derived oligodendrocyte progenitor cell transplants remyelinate and restore locomotion after spinal cord injury. *J Neurosci* 25:4694–4705.
14. Sharp J, Frame J, Siegenthaler M, Nistor G, Keirstead HS (2010) Human embryonic stem cell-derived oligodendrocyte progenitor cell transplants improve recovery after cervical spinal cord injury. *Stem Cells* 28:152–163.
15. Strauss S (2010) Geron trial resumes, but standards for stem cell trials remain elusive. *Nat Biotechnol* 28:989–990.
16. Takahashi K, Yamanaka S (2006) Induction of pluripotent stem cells from mouse embryonic and adult fibroblast cultures by defined factors. *Cell* 126:663–676.
17. Okita K, Ichisaka T, Yamanaka S (2007) Generation of germline-competent induced pluripotent stem cells. *Nature* 448:313–317.
18. Tsuji O, et al. (2010) Therapeutic potential of appropriately evaluated safe-induced pluripotent stem cells for spinal cord injury. *Proc Natl Acad Sci USA* 107:12704–12709.
19. Takahashi K, et al. (2007) Induction of pluripotent stem cells from adult human fibroblasts by defined factors. *Cell* 131:861–872.
20. Bregman BS (1987) Spinal cord transplants permit the growth of serotonergic axons across the site of neonatal spinal cord transection. *Brain Res* 431:265–279.
21. Saruhashi Y, Young W, Perkins R (1996) The recovery of 5-HT immunoreactivity in lumbosacral spinal cord and locomotor function after thoracic hemisection. *Exp Neurol* 139:203–213.
22. Kim D, et al. (1999) Direct agonists for serotonin receptors enhance locomotor function in rats that received neural transplants after neonatal spinal transection. *J Neurosci* 19:6213–6224.
23. Kobayashi NR, et al. (1997) BDNF and NT-4/5 prevent atrophy of rat rubrospinal neurons after cervical axotomy, stimulate GAP-43 and Talpha1-tubulin mRNA expression, and promote axonal regeneration. *J Neurosci* 17:9583–9595.
24. Krenz NR, Weaver LC (1998) Sprouting of primary afferent fibers after spinal cord transection in the rat. *Neuroscience* 85:443–458.
25. Krenz NR, Meakin SO, Krassioukov AV, Weaver LC (1999) Neutralizing intraspinal nerve growth factor blocks autonomic dysreflexia caused by spinal cord injury. *J Neurosci* 19:7405–7414.
26. Li S, Kim JE, Budel S, Hampton TG, Strittmatter SM (2005) Transgenic inhibition of Nogo-66 receptor function allows axonal sprouting and improved locomotion after spinal injury. *Mol Cell Neurosci* 29:26–39.
27. Springer JE, et al. (2010) The functional and neuroprotective actions of Neu2000, a dual-acting pharmacological agent, in the treatment of acute spinal cord injury. *J Neurotrauma* 27:139–149.
28. Beattie MS, et al. (1997) Endogenous repair after spinal cord contusion injuries in the rat. *Exp Neurol* 148:453–463.
29. Kim HM, Hwang DH, Lee JE, Kim SU, Kim BG (2009) Ex vivo VEGF delivery by neural stem cells enhances proliferation of glial progenitors, angiogenesis, and tissue sparing after spinal cord injury. *PLoS ONE* 4:e4987.
30. Yoshida H, et al. (2002) Platelet-activating factor enhances the expression of vascular endothelial growth factor in normal human astrocytes. *Brain Res* 944:65–72.
31. Mense SM, et al. (2006) Gene expression profiling reveals the profound upregulation of hypoxia-responsive genes in primary human astrocytes. *Physiol Genomics* 25: 435–449.
32. Hofstetter CP, et al. (2002) Marrow stromal cells form guiding strands in the injured spinal cord and promote recovery. *Proc Natl Acad Sci USA* 99:2199–2204.
33. Jones LL, Oudega M, Bunge MB, Tuszynski MH (2001) Neurotrophic factors, cellular bridges and gene therapy for spinal cord injury. *J Physiol* 533:83–89.
34. Brock JH, et al. (2010) Local and remote growth factor effects after primate spinal cord injury. *J Neurosci* 30:9728–9737.
35. Jakeman LB, Wei P, Guan Z, Stokes BT (1998) Brain-derived neurotrophic factor stimulates hindlimb stepping and sprouting of cholinergic fibers after spinal cord injury. *Exp Neurol* 154:170–184.
36. Tuszynski MH, et al. (1996) Nerve growth factor delivery by gene transfer induces differential outgrowth of sensory, motor, and noradrenergic neurites after adult spinal cord injury. *Exp Neurol* 137:157–173.
37. Tuszynski MH (1997) Gene therapy for nervous system disease. *Ann N Y Acad Sci* 835: 1–11.
38. Kitamura K, et al. (2007) Hepatocyte growth factor promotes endogenous repair and functional recovery after spinal cord injury. *J Neurosci Res* 85:2332–2342.
39. Abematsu M, et al. (2010) Neurons derived from transplanted neural stem cells restore disrupted neuronal circuitry in a mouse model of spinal cord injury. *J Clin Invest* 120:3255–3266.
40. Mitsui T, Shumsky JS, Lepore AC, Murray M, Fischer I (2005) Transplantation of neuronal and glial restricted precursors into contused spinal cord improves bladder and motor functions, decreases thermal hypersensitivity, and modifies intraspinal circuitry. *J Neurosci* 25:9624–9636.
41. Kim BG, Dai HN, Lynskey JV, McAtee M, Bregman BS (2006) Degradation of chondroitin sulfate proteoglycans potentiates transplant-mediated axonal remodeling and functional recovery after spinal cord injury in adult rats. *J Comp Neurol* 497: 182–198.
42. White TE, et al. (2010) Neuronal progenitor transplantation and respiratory outcomes following upper cervical spinal cord injury in adult rats. *Exp Neurol* 225:231–236.
43. Bonner JF, Blesch A, Neuhuber B, Fischer I (2010) Promoting directional axon growth from neural progenitors grafted into the injured spinal cord. *J Neurosci Res* 88: 1182–1192.
44. Schneider SP, Fyffe RE (1992) Involvement of GABA and glycine in recurrent inhibition of spinal motoneurons. *J Neurophysiol* 68:397–406.
45. Malcangio M, Bowery NG (1996) GABA and its receptors in the spinal cord. *Trends Pharmacol Sci* 17:457–462.
46. Kim DS, et al. (2010) Transplantation of gabaergic neurons from ES cells attenuates tactile hypersensitivity following spinal cord injury. *Stem Cells* 28:2099–2108.
47. Watanabe K, et al. (2004) Comparison between fetal spinal-cord- and forebrain-derived neural stem/progenitor cells as a source of transplantation for spinal cord injury. *Dev Neurosci* 26:275–287.
48. Ogawa D, et al. (2009) Evaluation of human fetal neural stem/progenitor cells as a source for cell replacement therapy for neurological disorders: Properties and tumorigenicity after long-term in vitro maintenance. *J Neurosci Res* 87:307–317.
49. Yan J, et al. (2007) Extensive neuronal differentiation of human neural stem cell grafts in adult rat spinal cord. *PLoS Med* 4:e39.
50. Fusaki N, Ban H, Nishiyama A, Saeki K, Hasegawa M (2009) Efficient induction of transgene-free human pluripotent stem cells using a vector based on Sendai virus, an RNA virus that does not integrate into the host genome. *Proc Jpn Acad, Ser B, Phys Biol Sci* 85:348–362.
51. Okita K, Nakagawa M, Hyenjong H, Ichisaka T, Yamanaka S (2008) Generation of mouse induced pluripotent stem cells without viral vectors. *Science* 322:949–953.
52. Zhou H, et al. (2009) Generation of induced pluripotent stem cells using recombinant proteins. *Cell Stem Cell* 4:381–384.
53. Warren L, et al. (2010) Highly efficient reprogramming to pluripotency and directed differentiation of human cells with synthetic modified mRNA. *Cell Stem Cell* 7: 618–630.
54. Rhee YH, et al. (2011) Protein-based human iPS cells efficiently generate functional dopamine neurons and can treat a rat model of Parkinson disease. *J Clin Invest* 121: 2326–2335.
55. Okita K, et al. (2011) A more efficient method to generate integration-free human iPS cells. *Nat Methods* 8:409–412.
56. Miura K, et al. (2009) Variation in the safety of induced pluripotent stem cell lines. *Nat Biotechnol* 27:743–745.
57. Scheff SW, Rabchevsky AG, Fugaccia I, Main JA, Lumpp JE, Jr. (2003) Experimental modeling of spinal cord injury: Characterization of a force-defined injury device. *J Neurotrauma* 20:179–193.

Human Molecular Genetics, 2011, Vol. 20, No. 23 **4530–4539**
doi:10.1093/hmg/ddr394
Advance Access published on September 7, 2011

Modeling familial Alzheimer's disease with induced pluripotent stem cells

Takuya Yagi[1], Daisuke Ito[1,*], Yohei Okada[2,3], Wado Akamatsu[2], Yoshihiro Nihei[1], Takahito Yoshizaki[1], Shinya Yamanaka[4], Hideyuki Okano[2] and Norihiro Suzuki[1]

[1]Department of Neurology, [2]Departments of Physiology and [3]Kanrinmaru Project, School of Medicine, Keio University, 35 Shinanomachi, Shinjuku-ku, Tokyo 160-8582, Japan and [4]Center for iPS Cell Research and Application, Kyoto University, Kyoto 606-8507, Japan

Received June 3, 2011; Revised August 1, 2011; Accepted August 29, 2011

Alzheimer's disease (AD) is the most common form of age-related dementia, characterized by progressive memory loss and cognitive disturbance. Mutations of presenilin 1 (*PS1*) and presenilin 2 (*PS2*) are causative factors for autosomal-dominant early-onset familial AD (FAD). Induced pluripotent stem cell (iPSC) technology can be used to model human disorders and provide novel opportunities to study cellular mechanisms and establish therapeutic strategies against various diseases, including neurodegenerative diseases. Here we generate iPSCs from fibroblasts of FAD patients with mutations in *PS1* (A246E) and *PS2* (N141I), and characterize the differentiation of these cells into neurons. We find that FAD–iPSC-derived differentiated neurons have increased amyloid β42 secretion, recapitulating the molecular pathogenesis of mutant presenilins. Furthermore, secretion of amyloid β42 from these neurons sharply responds to γ-secretase inhibitors and modulators, indicating the potential for identification and validation of candidate drugs. Our findings demonstrate that the FAD-iPSC-derived neuron is a valid model of AD and provides an innovative strategy for the study of age-related neurodegenerative diseases.

INTRODUCTION

Alzheimer's disease (AD) is one of the most common neurodegenerative disorders of the elderly, characterized by progressive memory disorientation and cognitive disturbance. The pathological profile of AD is neuronal loss in the cerebral cortex accompanied by massive accumulation of two types of amyloid fibril seeding senile plaques and hyperphosphorylated tau forming paired helical filaments. The amyloid fibril is mainly composed of β-amyloid (Aβ) peptides, the 40 and 42 amino acid forms (Aβ40 and Aβ42), that are derived by proteolytic cleavages from the amyloid precursor protein (APP) by β- and γ-secretase activity (1,2). According to the amyloid cascade hypothesis, a prevailing theory of AD pathology, accumulation of Aβ, mainly Aβ42, in the brain is the initiator of AD pathogenesis, subsequently leading to the formation of neurofibrillary tangles containing hyperphosphorylated tau protein, and consequently neuronal loss (3–5).

Presenilin 1 (*PS1*) and presenilin 2 (*PS2*) genes encoding the major component of γ-secretase have been identified as the causative genes for autosomal-dominant familial Alzheimer's disease (FAD). Mutations in the *PS1* gene, located on chromosome 14, occur most frequently in FAD (6,7). Ala246Glu (A246E) in *PS1* is a well-characterized FAD mutation that shows typical phenotypes of AD with complete penetrance. Mutations in the *PS2* gene on chromosome 1 are a relatively rare cause of FAD and are variably penetrant. Asn-141 substitutions by Ile (N141I) in the *PS2* gene was the first identified causative mutation of *PS2* in affected patients from the now famous Volga German families (8,9).

Mutations in the *PS1*, *PS2* and the *APP* gene account for most of the familial early onset cases of AD either by enhancing the production of pathological Aβ or especially Aβ42, which has a greater tendency to form fibrillary amyloid deposits. These findings support β-amyloid as the common initiating factor in AD in the amyloid cascade hypothesis (10,11). Both A246E in *PS1* and N141I in *PS2* are reported to induce

*To whom correspondence should be addressed at: Department of Neurology, School of Medicine, Keio University, 35 Shinanomachi, Shinjuku-ku, Tokyo 160-8582, Japan. Tel: +81 353633788; Fax: +81 333531272; Email: d-ito@jk9.so-net.ne.jp

elevation of Aβ42 levels in human plasma, patient-derived fibroblasts, forced-expressed cells and, in mice, showing strong toxicity (10–13).

Generation of human iPSCs provides a new method for elucidating the molecular basis of human disease (14,15). An increasing number of studies have employed disease-specific human iPSCs in neurological diseases, and a few have demonstrated disease-specific phenotypes to model the neurological phenotype (16–24). Here, we report the generation of iPSC from fibroblasts of FAD with the *PS1* mutation A246E and the *PS2* mutation N141I, and differentiation of these cells into neurons. We demonstrate that patient-derived differentiated neurons increase Aβ42 secretion, recapitulating the pathological mechanism of FAD with *PS1* and *PS2* mutations. Our findings demonstrate that the FAD–iPSC-derived neuron is a valid model for studying AD, and provides important clues for the identification and validation of candidate drugs.

RESULTS

Generation of iPSC with presenilin mutations

We established two clones of iPSCs with the *PS1* mutation, A246E (PS1-2 iPSC and PS1-4 iPSC) and with the *PS2* mutation, N141I (PS2-1 iPSC and PS2-2 iPSC) by retroviral transduction of primary human fibroblasts with the five factors OCT4, SOX2, KLF4, LIN28 and NANOG. Fibroblasts were obtained from the Coriell Cell Repository (AG07768 and AG09908). The 201B7 iPSC line (14) and the sporadic Parkinson disease (PD)-derived iPSC lines (PD01-25 and 26) were reprogrammed by an original method (14) with four transcription factors (OCT4, SOX2, KLF4 and cMYC) and were used as the controls in this study. Genotyping of the established iPSC lines was confirmed by PCR–RFLP and sequencing (Fig. 1A and B). All PS1 and PS2 iPSC clones demonstrated typical characteristics of pluripotent stem cells: similar morphology to ESCs, expression of pluripotent markers including Tra-1-60, Tra-1-81, SSEA3 and SSEA4 (Fig. 1C), silencing of retroviral transgenes and reactivation of genes indicative of pluripotency (Fig. 1D). The differentiation ability of PS1 and PS2 iPSC was also confirmed *in vivo* by teratoma formation (Fig. 2), and *in vitro* by the formation of three germ layers via embryoid bodies (Supplementary Material, Fig. S1). To validate our reprogramming technique, we performed comprehensive analysis of two PS2 iPSCs. Heat map analysis showed that global gene expression profiles, including the critical genes for pluripotency, were similar between the iPSC lines established with four transcription factors (201B7 and PD01-25) and the PS2 iPSC clones established with five transcription factors (Supplementary Material, Fig. S2). In addition, there were no significant differences in the expression of AD-related molecules between PS2 iPSCs and control iPSCs (Supplementary Material, Fig. S3). Array comparative genomic hybridization (aCGH) analysis on PS2-1, PS2-2 iPSC and AG09908 fibroblasts showed that the total number of copy number aberrations were 52, 61 and 102 out of ~17 000 locations, respectively (Supplementary Material, Table S1), and no aberrations were detected in *APP*, *PS1* and *PS2* genes.

Differentiation of PS1 iPSC and PS2 iPSC into neurons

Differentiation of FAD patient-specific iPSCs towards neurons enables modeling the disease pathogenesis *in vitro*. To establish whether the presenilin mutations may affect neuronal differentiation, both PS1 and PS2 iPSC lines, as well as control iPSC lines, were induced to differentiate into neural cells (25,26), and cultured on Matrigel-coated dishes for 2 weeks to induce terminal differentiation (Fig. 3). We confirmed neuronal differentiation by the expression of neuronal markers, βIII-tubulin, and MAP-2 (Fig. 3A and B). As shown in Figure 3C, no obvious differences in the ability to generate neurons (~80% βIII-tubulin-positive cells) were observed among control, PS1 and PS2 iPSCs. This indicated that PS1 and PS2 iPSCs can generate neurons with almost the same efficiency as the control iPSCs, suggesting these presenilin mutations may have no significant effect on neuronal differentiation.

Production of Aβ secreted from iPSCs-derived neurons

To analyze the functional aspects of FAD, we investigated Aβ secretion from iPSC or iPSC-derived neurons. The Aβ secretion in the conditioned medium from control iPSC, PS1 iPSC and PS2 iPSC was very low; Aβ42 secretion especially was below the detection sensitivity. We therefore could not compare the ratio of Aβ42 to Aβ40 among iPSC lines. However, the Aβ secretion in the conditioned medium from the iPSCs-derived neurons was increased and measurable, indicating that Aβ secretion could undergo significant fluctuation during differentiation. Although the levels of Aβ42 and Aβ40 in the medium showed some clonal variation (Fig. 4A), possibly depending on the rate of cell growth and passage number, the ratio of Aβ42 to Aβ40 was significantly elevated in the PS1 and PS2 iPSCs-derived neurons, compared with the controls (Fig. 4B). Thus, PS1 and PS2 iPSCs show that living neurons derived from patients with the presenilin mutations ending at residue 42 that are linked to FAD secrete more Aβ. This result is compatible with previous evidences based on patients' plasma, fibroblasts and forced-expressed cells (10–13).

To explore recapitulation of key pathological events in AD, we investigated whether FAD-iPSC-derived differentiated neurons exhibit abnormal accumulation of tau and performed an immunoblot analysis of lysates of FAD-iPSC-derived neurons with anti-tau antibody. However, as shown in Supplementary Material, Figure S4, no abnormal tau protein accumulation or tangle formation was detected in the FAD-derived neurons, indicating that recapitulation of tauopathy is difficult to observe during the short culture period (2 weeks) in the present protocol.

Pharmacological response to γ-secretase inhibitors in PS1 iPSC- and PS2 iPSC-derived neurons

To evaluate the capacity of pharmacological drug screening in iPSC technology, we assessed whether inhibitors could affect the secretion of Aβ in PS1 and PS2 iPSCs-derived neurons. We first examined the secretion of Aβ from PS1-4 and PS2-2 iPSCs-derived neurons in the presence of Compound E, a

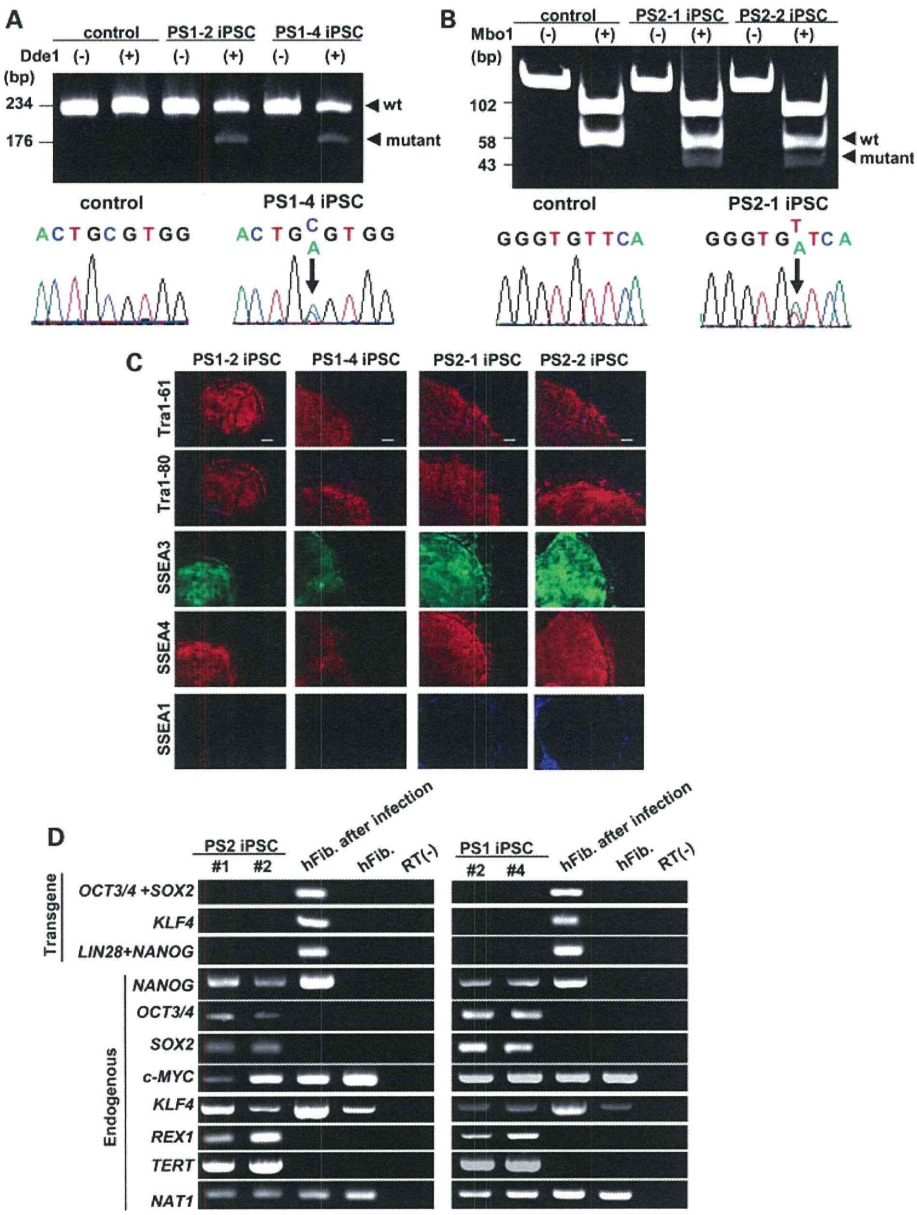

Figure 1. Generation of PS1 and PS2 iPSC from patient fibroblasts. (**A**) Genotypic analysis of PS1 iPSC by PCR–RFLP and sequencing. A246E genotyping by PCR–RFLP was performed with restriction enzyme *Dde*I. The A246E mutation results in fragments of 176 and 58 bp, whereas the control fragment has 234 bp. (**B**) Genotypic analysis of PS2 iPSC by PCR–RFLP and sequencing. N141I genotyping by PCR–RFLP was performed with restriction enzyme *Mbo*I. The N141I mutation results in fragments of 102, 58 and 43 bp, whereas the control has fragment lengths of 102 and 58 bp. (**C**) Both PS1 and PS2 iPSC lines exhibit markers of pluripotency. All iPSCs express pluripotency markers including Tra-1-60, Tra-1-81, SSEA3 and SSEA4. Nuclei were stained with 4,6-diamidino-2-phenylindole (DAPI). Bar = 200 μm. (**D**) RT–PCR analysis of the transgenes OCT3/4, SOX2, KLF4 and the endogenous hESC marker genes. Patient fibroblasts 6 days after the transduction with the retroviruses are positive for the transgenes.

potent γ-secretase inhibitor (27) (Fig. 5A and B). With the addition of 10 and 100 nM Compound E, the production of both Aβ42 and Aβ40 was suppressed in a dose-dependent manner, when compared with untreated in both of PS1-4 and PS2-2 iPSC-derived neurons. Next, we assessed the ability of Compound W, a selective Aβ42-lowering agent, to modulate γ-secretase-mediated APP cleavage (28) (Fig. 5A and B). As expected, the addition of Compound W caused a drastic decrease in the ratio of Aβ42 to Aβ40 in both neurons.

We also determined the effect of these compounds on the proteolytic processing that causes a release of an intracellular domain of Notch, another γ-secretase substrate. Western blotting using the anti-S3 cleaved Notch1-specific antibody demonstrated that productions of Notch intracellular domain